AD_____

Award Number: MIPR9LDATM9117

TITLE: Breast Microcalcification Detection Using Super-Resolution Ultrasound Image Reconstruction

PRINCIPAL INVESTIGATOR: Lianjie Huang

CONTRACTING ORGANIZATION: Los Alamos national Laboratory
Los Alamos, NM 87545

REPORT DATE: September 2010

TYPE OF REPORT: Annual

PREPARED FOR: U.S. Army Medical Research and Materiel Command
Fort Detrick, Maryland 21702-5012

REPORT DOCUMENTATION PAGE

Form Approved
OMB No. 0704-0188

1. REPORT DATE *(DD-MM-YYYY)*	**2. REPORT TYPE**	**3. DATES COVERED** *(From - To)*
01-09-2010	Annual	1 Sep 2009 - 31 Aug 2010

4. TITLE AND SUBTITLE
Breast Microcalcification Detection Using Super-Resolution Ultrasound Image Reconstruction

5a. CONTRACT NUMBER
MIPR9LDATM9117

5b. GRANT NUMBER

5c. PROGRAM ELEMENT NUMBER

6. AUTHOR(S)
Lianjie Huang

5d. PROJECT NUMBER

5e. TASK NUMBER

5f. WORK UNIT NUMBER

7. PERFORMING ORGANIZATION NAME(S) AND ADDRESS(ES)
Los Alamos National Laboratory, Los Alamos, NM 87545

8. PERFORMING ORGANIZATION REPORT NUMBER

9. SPONSORING / MONITORING AGENCY NAME(S) AND ADDRESS(ES)
U.S. Army Medical Research and Materiel Command
Fort Detrick, Maryland 21702-5012

10. SPONSOR/MONITOR'S ACRONYM(S)

11. SPONSOR/MONITOR'S REPORT NUMBER(S)

12. DISTRIBUTION / AVAILABILITY STATEMENT
Approved for public release; distribution unlimited

13. SUPPLEMENTARY NOTES

14. ABSTRACT
We explore the use of the super-resolution ultrasound imaging method for detecting breast microcalcifications. We validate and test its imaging capability using numerical breast phantom data. We also study breast microcalcification detection using wave-equation reflection/migration imaging. Wave-equation reflection/migration imaging can effectively reduce image speckles by properly handling ultrasound scattering/diffraction from breast heterogeneities during image reconstruction. We construct numerical breast phantoms using *in vivo* breast images, and use a time-domain finite-difference wave-equation scheme to generate ultrasound data scattered from inclusions that mimic microcalcifications. Our numerical phantom studies show that microcalcifications can be detected at full spatial resolution using both the super-resolution ultrasound imaging and wave-equation migration/reflection imaging methods.

15. SUBJECT TERMS
Breast microcalcification, super-resolution imaging, ultrasound, wave-equation reflection/migration imaging.

16. SECURITY CLASSIFICATION OF:			**17. LIMITATION OF ABSTRACT**	**18. NUMBER OF PAGES**	**19a. NAME OF RESPONSIBLE PERSON**
a. REPORT	**b. ABSTRACT**	**c. THIS PAGE**			**19b. TELEPHONE NUMBER** *(include area code)*
U	U	U	UU	21	USAMRMC

Table of Contents

Introduction

This research is to study a super-resolution ultrasound imaging method for breast microcalcification detection. The first-years work is primarily focused on Task 1 (Aim 1): Refine, validate and test a super-resolution image reconstruction algorithm using numerical breast phantom data. We use numerical breast phantom data to validate and test the imaging capability of the super-resolution ultrasound imaging method for detecting breast microcalcifications. The super-resolution ultrasound imaging uses the singular value decomposition and a factorization scheme to achieve an image resolution that is not possible for conventional ultrasound imaging. In addition, we study breast microcalcification detection using wave-equation reflection/migration imaging and numerical breast phantoms. Wave-equation reflection/migration imaging can effectively reduce image speckles by properly handling ultrasound scattering/diffraction from breast heterogeneities during image reconstruction. Wave-equation reflection imaging employs a solution to the acoustic-wave equation in heterogeneous media to backpropagate ultrasound scattering/diffraction waves to scatters and reconstruct images of heterogeneities. We construct numerical breast phantoms using *in vivo* breast images, and use a time-domain finite-difference wave-equation scheme to generate ultrasound data scattered from inclusions that mimic microcalcifications. Our numerical phantom studies demonstrate that microcalcifications can be detected at full spatial resolution using both the super-resolution ultrasound imaging and wave-equation migration/reflection imaging methods.

Body

During the first year of the project work, we primarily focused on Task 1 (Aim 1): Refine, validate and test super-resolution ultrasound image reconstruction (SRUI) algorithm, including

a. Refine the theory;
b. Develop the computer program;
c. Generate numerical phantom data;
d. Image reconstruction with numerical phantom data.

We refine the SRUI method by extending it for heterogeneous media. This is important for *in vivo* applications. We study the SRUI method for imaging mimic breast calcifications situated in different masses within heterogeneous breasts. Our preliminary results using numerical breast phantom data demonstrate that the SRUI method has the potential to detect microcalcifications in heterogeneous breasts.

We develop a new computer program of the SRUI algorithm. Our super-resolution ultrasound image reconstruction is based on a factorization method to reconstruct the shape of a scatterer using the spectral data of the far field operator, i.e. its eigenvalues and eigenfunctions (Kirsch 1998). Our SRUI algorithm was first developed using MATLAB.We develop a new program code of the SRUI algorithm using Fortran to significantly improve its computational efficiency. The computational speed of the new code is approximately two orders of magnitudes faster than that of the MATLAB code.

We construct numerical breast phantoms based on *in vivo* breast images. Breast microcalcifications can be found within a water cyst or an oil cyst occasionally, and within a cancerous mass.

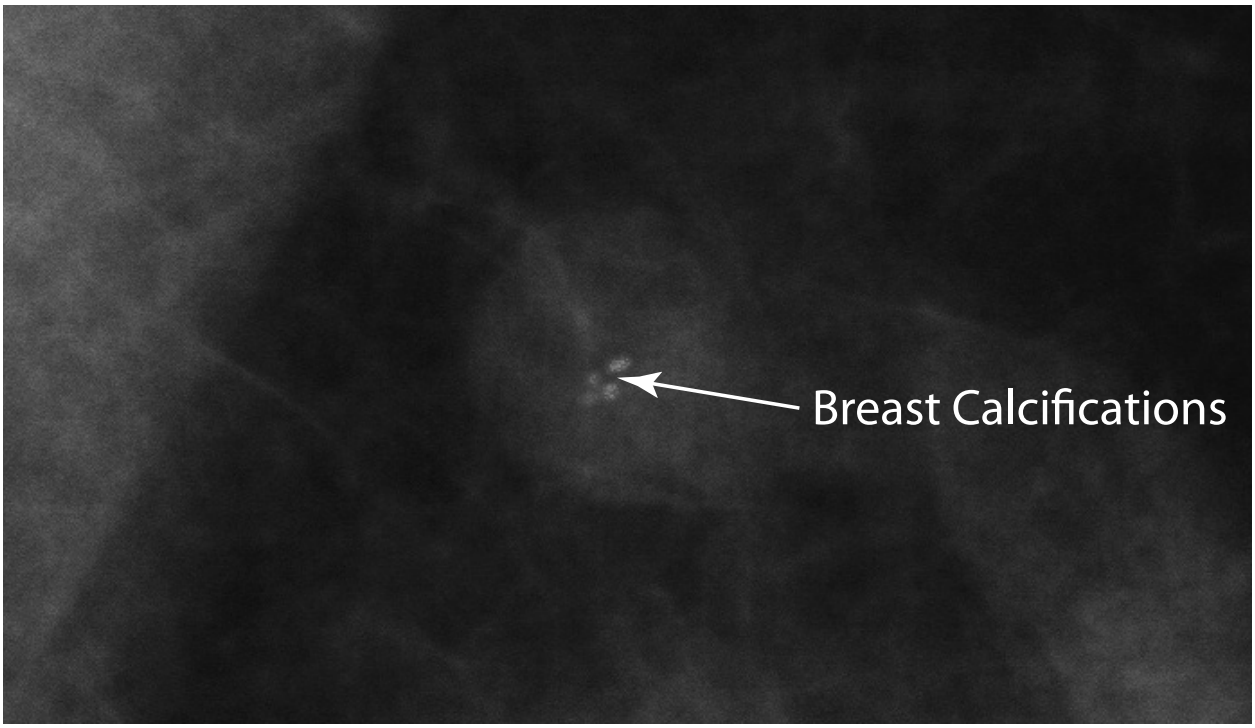

Figure 1: A mammogram showing breast calcifications as the bright spots within a cyst.

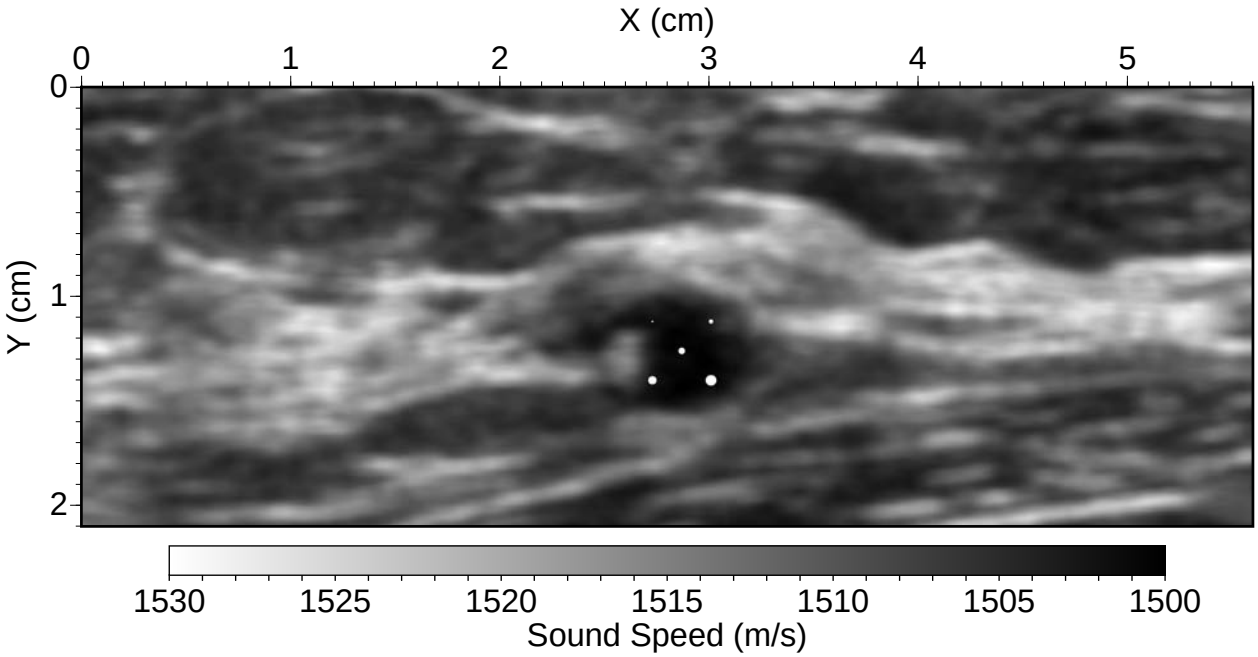

Figure 2: The sound speed profile of a numerical breast phantom containing five microcalcifications with diameters of 0.08 mm, 0.20 mm, 0.32 mm, 0.40 mm, and 0.52 mm within a cyst. The numerical phantom is constructed based on an *in vivo* ultrasound breast image. The embedded microcalcifications are shown as the bright spots.

Breast microcalcifications within a cyst are likely benign, and those within a cancerous mass could be malignant.

Figure 1 is a mammogram showing breast calcifications within a cyst. We construct a numerical breast phantom based on Fig. 1, and insert five microcalcifications inside the cyst to study the imaging capability of the SRUI method for detecting breast microcalcifications. The constructed numerical breast phantom is shown in Fig. 2.

We generate synthetic ultrasound data scattered from the mimic breast microcalcifications in Fig. 2 using a finite-difference time-domain method to solve the acoustic-wave equation in heterogeneous media. The phantom is scanned at its top surface using a linear ultrasound array with a size of 5.6 cm and a central frequency of 5 MHz. The central wavelength of the probing ultrasound is approximately 0.3 mm. Therefore, the sizes of the embedded microcalcifications are smaller than or in the same order as the ultrasound wavelength, resulting in significant ultrasound diffraction from the microcalcifications. To satisfy the spatial sampling criterion of ultrasound data (or two receivers per wavelength) to avoid image aliasing during image reconstruction, it requires at least 373 elements in the linear transducer array.

We conduct image reconstruction with the numerical phantom data to validate and test our SRUI algorithm for detecting breast microcalcifications.

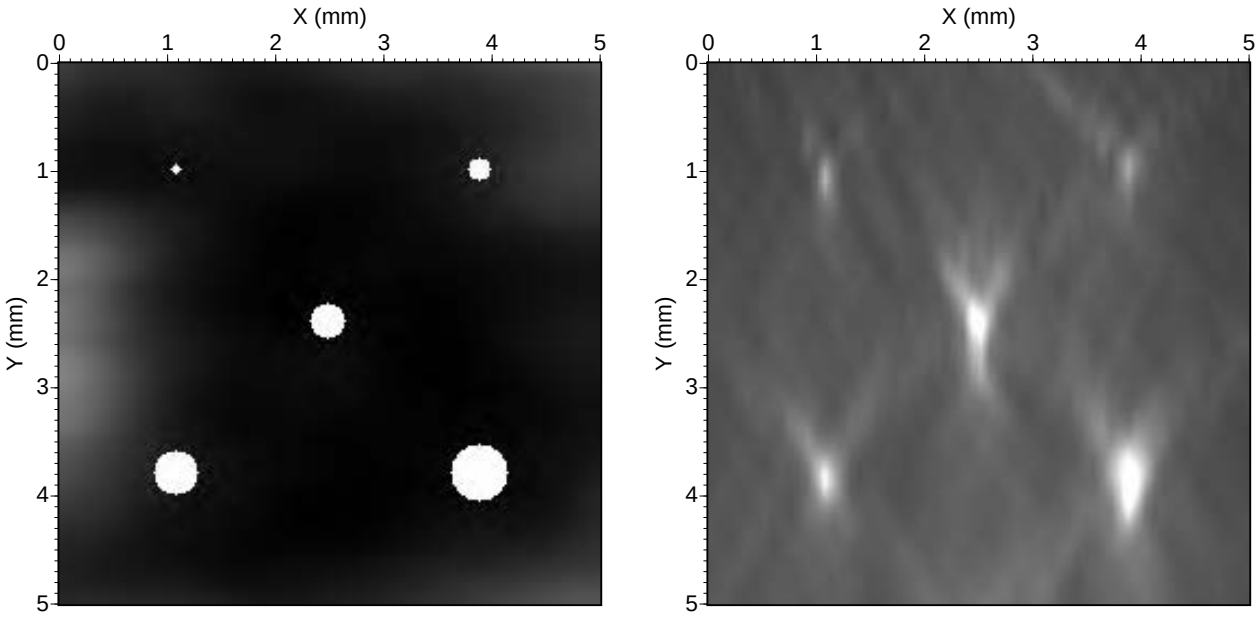

(a) Magnified view of the region with five breast microcalcifications in Fig. 2

(b) Super-resolution imaging with 351 transducer elements (∼1.9 elements per wavelength)

Figure 3: Magnified view of the region with embedded microcalcifications in Fig. 2 and the corresponding super-resolution imaging result obtained using a linear ultrasound array with 351 elements. All five microcalcifications can be clearly identified.

Figure 3(a) is the magnified view of the region with the embedded breast microcalcifications within a cyst in Fig. 2. Our super-resolution image of the embedded breast microcalcifications obtained with 351 transducer elements (or 1.9 elements per wavelength) is displayed in Fig. 3(b).

This numerical study shows that microcalcifications in a heterogeneous breast can be clearly detected using our super-resolution ultrasound imaging.

In addition to super-resolution imaging, we also study wave-equation migration/reflection imaging for breast microcalcification detection. Breast microcalcifications can be seen in malignant cancerous masses. We construct a numerical breast phantom in Fig. 4 from an *in vivo* image with malignant calcifications. Again, five microcalcifications with sizes ranging from 0.08 mm to 0.52 mm are embedded into the cancerous mass. We use the same finite-difference wave-equation scheme to generate synthetic data of ultrasound diffraction from the embedded microcalcifications in Fig. 4. The size and the central frequency of the linear transducer array that scans the breast phantom at its top surface are the same as those of the previous numerical example.

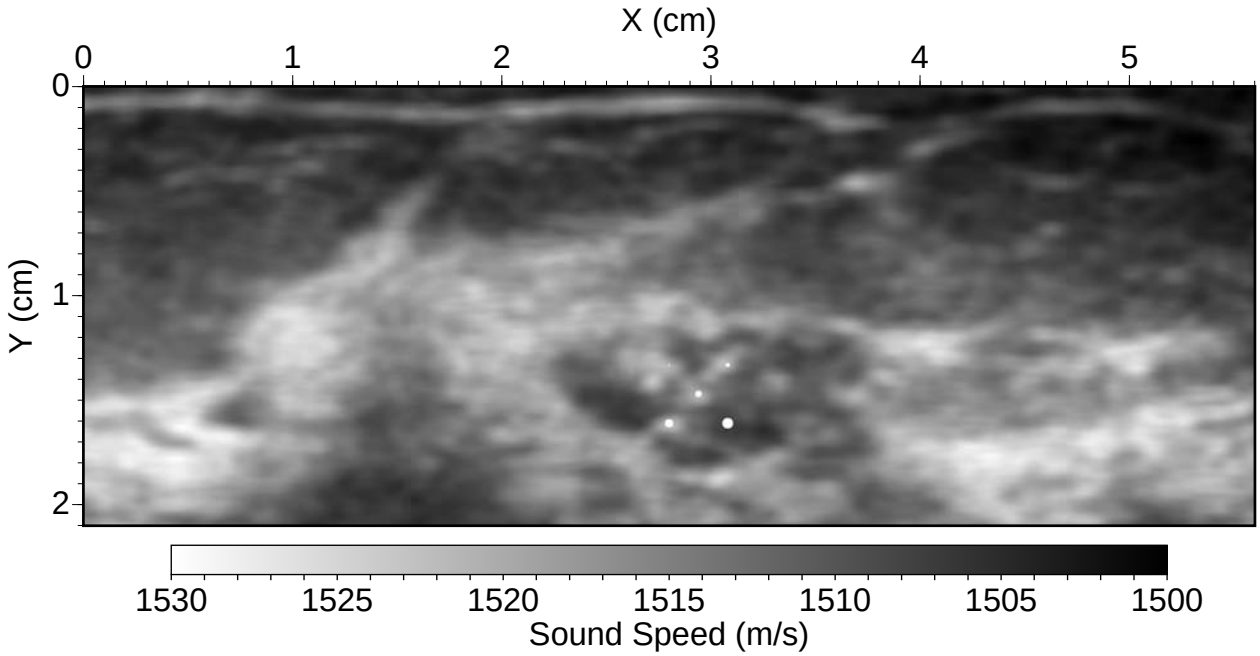

Figure 4: The sound speed profile of a numerical breast phantom containing five microcalcifications with diameters of 0.08 mm, 0.20 mm, 0.32 mm, 0.40 mm, and 0.52 mm within a cancer mass. The numerical phantom is constructed based on an *in vivo* ultrasound breast image.

We perform wave-equation reflection/migration imaging with the synthetic ultrasound data from the numerical breast phantom in Fig. 4. The magnified view of the region with the microcalcifications in Fig. 4 is shown in Fig. 5(a), and the corresponding wave-equation reflection imaging result with 401 transducer elements are displayed in Fig 5(b). All breast microcalcifications are clearly reconstructed with our wave-equation reflection imaging.

More detailed descriptions of the work on super-resolution ultrasound image reconstruction and wave-equation reflection/migration imaging with numerical breast phantoms can be found in Huang et al. (2010) (See Appendix).

In addition to work for Task 1 (Aim 1), we have initiated the work for Task 2 (Aim2). We have purchased an ultrasound phantom that is designed for testing imaging resolution. Los Alamos National Laboratory provided funding to purchase a new synthetic aperture ultrasound scanner for this study. We will acquire phantom and *in vivo* patient data using the new ultrasound scanner,

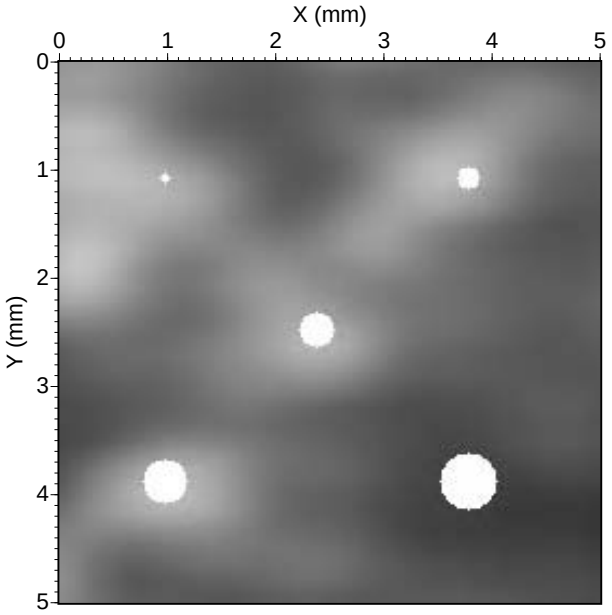

(a) Magnified view of the region with five breast microcalcifications shown in Fig. 4.

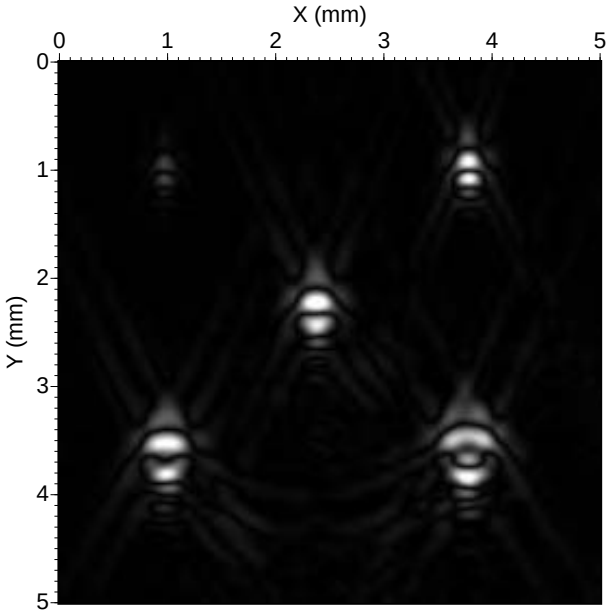

(b) Wave-equation reflection imaging with 401 transducer elements ($\sim$2.1 elements per wavelength)

Figure 5: Magnified view of the region with embedded microcalcifications in Fig. 4 and the corresponding wave-equation reflection imaging result obtained with 401 transducer elements of the linear ultrasound array. All microcalcifications are well imaged.

and use our super-resolution ultrasound imaging and wave-equation reflection imaging methods to conduct image reconstruction. Finally, the University of New Mexico has developed clinical protocols for patient scans.

Key Research Accomplishments

1. We have shown using numerical breast phantom data that our super-resolution ultrasound imaging method has the capability to detect microcalcifications in heterogeneous breasts.
2. We have numerically demonstrated that wave-equation reflection/migration imaging is another potential imaging method for detecting breast microcalcifications.

Reportable Outcomes

Here is a list of reportable outcomes that have resulted from this research:

1. Two proceeding papers were published (Huang et al. 2010; Huthwaite et al. 2010)
2. A poster was presented at the 2010 SPIE Medical Imaging Meeting. The poster received the *Cum Laude* Poster Award.

3. An abstract was submitted to the 2011 SPIE Medical Imaging Meeting, and was accepted.
4. Two abstracts were submitted to the 2011 AIUM Annual Conference.
5. Additional funding was obtained from Los Alamos National Laboratory to purchase a new synthetic ultrasound scanner to support this research.

Conclusions

We have developed and tested a super-resolution ultrasound imaging method and a wave-equation reflection/migration imaging method for breast microcalcification detection. We have demonstrated using numerical breast phantoms that both the super-resolution imaging with the factorization method and wave-equation reflection imaging can clearly image breast microcalcifications in heterogeneous breasts. Our numerical phantom studies have shown that both the super-resolution imaging with the factorization method and wave-equation reflection/migration imaging have great potential for clinical breast microcalcification detection.

References

Huang, L., Simonetti, F., Huthwaite, P., Rosenberg, R., and Williamson, M., 2010, Detecting breast microcalcifications using super-resolution and wave-equation ultrasound imaging: A numerical phantom study SPIE, Ultrasonic Imaging, Tomography, and Therapy, 762919–1–10.

Huthwaite, P., Simonetti, F., and Huang, L., 2010, The different structural scales of the breast and their impact on time-of-flight and diffraction tomography SPIE, Ultrasonic Imaging, Tomography, and Therapy, 76290L–1–8.

Kirsch, A., 1998, Characterization of the shape of a scattering obstacle using the spectral data of the far field operator: Inverse Problems, **14**, 1489–1512.

Appendices

Enclosed is the paper: Huang, L., Simonetti, F., Huthwaite, P., Rosenberg, R., and Williamson, M., 2010, Detecting breast microcalcifications using super-resolution and wave-equation ultrasound imaging: A numerical phantom study SPIE, Ultrasonic Imaging, Tomography, and Therapy, 762919-1-10.

Detecting breast microcalcifications using super-resolution and wave-equation ultrasound imaging: A numerical phantom study

Lianjie Huang[a], Francesco Simonetti[b], Peter Huthwaite[b],
Robert Rosenberg[c], and Michael Williamson[c]

[a]Los Alamos National Laboratory, Los Alamos, NM 87545
[b]Imperial College London, London SW7 2AZ, UK
[c]Department of Radiology, University of New Mexico, Albuquerque, NM 87131

ABSTRACT

Ultrasound image resolution and quality need to be significantly improved for breast microcalcification detection. Super-resolution imaging with the factorization method has recently been developed as a promising tool to break through the resolution limit of conventional imaging. In addition, wave-equation reflection imaging has become an effective method to reduce image speckles by properly handling ultrasound scattering/diffraction from breast heterogeneities during image reconstruction. We explore the capabilities of a novel super-resolution ultrasound imaging method and a wave-equation reflection imaging scheme for detecting breast microcalcifications. Super-resolution imaging uses the singular value decomposition and a factorization scheme to achieve an image resolution that is not possible for conventional ultrasound imaging. Wave-equation reflection imaging employs a solution to the acoustic-wave equation in heterogeneous media to backpropagate ultrasound scattering/diffraction waves to scatters and reconstruct images of heterogeneities. We construct numerical breast phantoms using *in vivo* breast images, and use a finite-difference wave-equation scheme to generate ultrasound data scattered from inclusions that mimic microcalcifications. We demonstrate that microcalcifications can be detected at full spatial resolution using the super-resolution ultrasound imaging and wave-equation reflection imaging methods.

Keywords: Breast microcalcification, diffraction, factorization, reflection, scattering, super-resolution imaging, ultrasound imaging, wave equation.

1. INTRODUCTION

Microcalcifications, tiny specks of mineral deposits (calcium), are the first sign of breast cancer in more than 30% of all cases. For example, ductal carcinoma in situ (DCIS) represents approximately 20% of all breast cancers detected by mammography, and approximately 95% of all DCIS is diagnosed because of mammographically detected microcalcifications. Breast microcalcifications often occur as one of two types: calcium oxalate dihydrate or calcium hydroxyapatite. Their sizes range approximately from 0.1 mm to 0.5 mm. They can be scattered throughout the mammary gland, or occur in clusters. Breast microcalcifications may or may not be associated with a tumor and, therefore, they must be detected and characterized accurately according to their size, number, distribution, and morphology to determine if they are benign or malignant. Multiple (three to five) microcalcifications within an area of 5 to 10 mm define a cluster of microcalcifications. The characteristics of benign calcifications include smooth contours, high uniform density, evenly scattered and homogeneous, sharply outlined spherical or oval shapes, bilateral and evenly scattered following the course of the ducts throughout much of the parenchyma, ring-like, hollow, eggshell like, and large and irregular sizes. The three basic forms of malignant calcifications are casting-type, granular-type and powderish calcifications.[1] Breast microcalcifications have no symptoms that a woman could notice herself, like a lump.

High-resolution imaging of breast microcalcifications is critically important for reliably detecting and characterizing the benign and malignant calcifications. X-ray mammography is the only imaging modality routinely used for detecting breast microcalcifications.[2–4] However, it is relatively less effective in women with dense breasts, especially in young women.[5,6] Digital mammography optimizes microcalcification detection using image processing. It has been demonstrated that digital

Send correspondence to Lianjie Huang: ljh@lanl.gov

Medical Imaging 2010: Ultrasonic Imaging, Tomography, and Therapy, edited by Jan D'hooge, Stephen A. McAleavey,
Proc. of SPIE Vol. 7629, 762919 · © 2010 SPIE · CCC code: 1605-7422/10/$18 · doi: 10.1117/12.844459

mammography has at least the equal detection performance of malignant microcalcifications compared to the screen-film mammography.[4,7]

Ultrasound imaging could be an attractive alternative tool for breast microcalcification detection. However, current clinical ultrasound imaging cannot detect microcalcification due its low image resolution and speckle. Breast microcalcifications are invisible within the noisy echo texture of either cancerous masses or ductal carcinoma in situ.[8–11] To overcome these limitations, some alternate techniques have been developed.[9,12,13] Current ultrasound imaging can only reliably detect large calcifications of several millimeters in size.

Super-resolution imaging with the factorization method has recently been developed to greatly improve ultrasound image resolution.[14,15] The super-resolution means that the image resolution will be much higher (one order of magnitude higher) than that of conventional imaging techniques. The super-resolution imaging with the factorization method is based on singular value decomposition of the so-called multistatic matrix obtained by measuring all the possible transmit-receive pairs across the aperture of a linear ultrasound array. Only the singular values above the noise threshold are used for image reconstruction, leading to partial noise suppression and high-resolution images with fewer speckles. The method makes use of the full waveform of ultrasound data including multiple scattering, as well as a factorization scheme[16] to achieve an image resolution that is not possible for conventional ultrasound imaging. Super-resolution imaging could remedy current deficiencies of clinical ultrasound in breast microcalcification detection.

An effective approach to image speckle reduction and image resolution improvement is using wave-equation reflection/migration imaging to properly account for ultrasound scattering/diffraction from breast heterogeneities during image reconstruction.[17–20] Sound speeds and densities of breast tissue are inhomogeneous,[21] and those of breast microcalcifications with sizes range from 0.1–0.5 mm are much higher than the surrounding tissues. These differences in mechanical properties result in ultrasound scattering. Because the sizes of breast microcalcifications are smaller than or in the order of the wavelength of probing ultrasound, diffraction waves dominate ultrasound scattering from microcalcifications. Most ultrasound imaging is based on the ray theory that is asymptotic approximation of ultrasound wave propagation in the infinite frequency limit, and cannot correctly deal with ultrasound diffraction. Only wave theory-based ultrasound imaging can accurately focus diffraction wavefields back to where they are generated so as to reconstruct images of scatters. Therefore, wave-equation reflection imaging could be a promising tool for breast microcalcification detection.

We explore the capabilities of the super-resolution imaging and wave-equation reflection imaging methods for breast microcalcification detection using numerical breast phantoms. Microcalcifications can be found in different breast tissues, such as cancerous masses or cysts. We build two numerical breast phantoms for this study: one containing microcalcifications within a cyst and the other with microcalcifications inside a cancerous mass. The heterogeneous distributions of the sound speed and density of the phantoms are constructed based on *in vivo* patient breast images. A finite-difference scheme to solve the acoustic-wave equation in heterogeneous media is used to generate numerical ultrasound diffraction data scattered from microcalcifications. We then conduct image reconstructions of breast microcalcifications using the super-resolution imaging and wave-equation reflection imaging methods. We show that the super-resolution imaging and wave-equation reflection imaging have great potential for breast microcalcification detection.

2. METHODOLOGY

Both the super-resolution imaging and wave-equation reflection imaging are based on the solutions of acoustic-wave equation in heterogeneous media. The super-resolution imaging with the factorization method was proposed by Kirsch[16] to reconstruct images of scatterer shapes. The wave-equation reflection imaging backpropagate/migrate received ultrasound wavefields to spatial locations where ultrasound scattering wavefields are generated.

2.1 Super-resolution imaging with the factorization method

Kirsch[16] proposed a factorization method to reconstruct the shape of a scatterer using the spectral data of the far field operator, i.e. its eigenvalues and eigenfunctions. The imaging condition of the factorization method at imaging point $\mathbf{z}$ is given by[14,15]

$$I(\mathbf{z}) = \left(\sum_{i=1}^{\infty} \frac{1}{|\mu_i|} \left| \langle g | v^i \rangle \right|^2 \right)^{-1}, \tag{1}$$

where I is the image, μ_i and v^i are the eigenvalue and eigenfunction of the far field T-matrix operator, respectively, and g is defined as

$$g(k\hat{\mathbf{r}}) = e^{-ik\hat{\mathbf{r}}\cdot\mathbf{z}}, \tag{2}$$

with k being the wavenumber of the probing plane wave, and $\hat{\mathbf{r}}$ being the propagation direction of a scattering wave at the receiver.

Ultrasound data always contain some noise. Only the eigenvalues above the noise threshold are used for image reconstruction in Eq. (1). Subwavelength image resolution can be achieved using the factorization method in Eq. (1).[15]

2.2 Wave-equation reflection imaging

The acoustic-wave equation in heterogeneous media can be decomposed into two one-way wave equations describing wave propagation in opposite directions. These one-way wave equations in the frequency-space domain are give by

$$\frac{\partial U(x,z;\omega)}{\partial z} = \pm i\, Q(x,z;\omega)\, U(x,z;\omega), \tag{3}$$

where $\pm$ are for waves propagating in opposite directions, U is the ultrasound wavefield, ω is the circular frequency, $(x,\ z)$ is the space location, and Q is an operator defined by

$$Q \equiv \sqrt{\frac{\omega^2}{c^2(x,z)} + \frac{\partial^2}{\partial x^2}} = \frac{\omega}{c(x,z)} R, \tag{4}$$

where c is the sound speed, and R is the square-root operator given by

$$R \equiv \sqrt{1 - X^2}, \tag{5}$$

with

$$X^2 \equiv -\frac{c^2}{\omega^2}\frac{\partial^2}{\partial x^2}. \tag{6}$$

The formal solution of Eq. (3) is

$$U(x,z+\Delta z;\omega) = \exp\left\{\pm i \int Q\, dz\right\} U(x,z;\omega), \tag{7}$$

which extrapolates ultrasound wavefield U from the depth level at z to the next depth level at $z+\Delta z$. Different approaches have been developed to numerically solve Eq. (7).[17,19,20] Wave-equation ultrasound reflection imaging uses the formal solution (7) for wavefield continuation to reconstruct images of breast heterogeneities including microcalcifications.

3. IMAGING OF BREAST MICROCALCIFICATIONS

We conduct numerical studies of super-resolution imaging and wave-equation ultrasound reflection imaging for detecting breast microcalcifications situated in different host tissues, including a cyst and a cancerous mass. Breast microcalcifications within a cyst are likely benign, and those within a cancerous mass could be malignant. We build numerical breast phantoms based on *in vivo* breast images, generate synthetic ultrasound diffraction data emerging from breast microcalcifications, and study the imaging capabilities of the super-resolution imaging and wave-equation reflection imaging for detecting breast microcalcifications.

3.1 Breast microcalcifications within a cyst

Breast microcalcifications can be found within a water cyst or an oil cyst occasionally. Figure 1 is a mammogram showing breast calcifications within a cyst. We construct a numerical breast phantom based on Fig. 1, insert five microcalcifications inside the cyst. Fig. 2 is the sound speed profile of the phantom. The breast sound speed varies from 1500 m/s to 1530 m/s, and the sound speed of the microcalcifications is 1800 m/s. The sizes of microcalcifications range from 0.08 mm to 0.52 mm. The phantom is scanned at the top surface of the phantom using a linear ultrasound array with a size of 5.6 cm and a central frequency of 5 MHz. The central wavelength of the probing ultrasound is approximately 0.3 mm. Therefore, the sizes of the embedded microcalcifications are smaller than or in the order of the ultrasound wavelength, resulting in

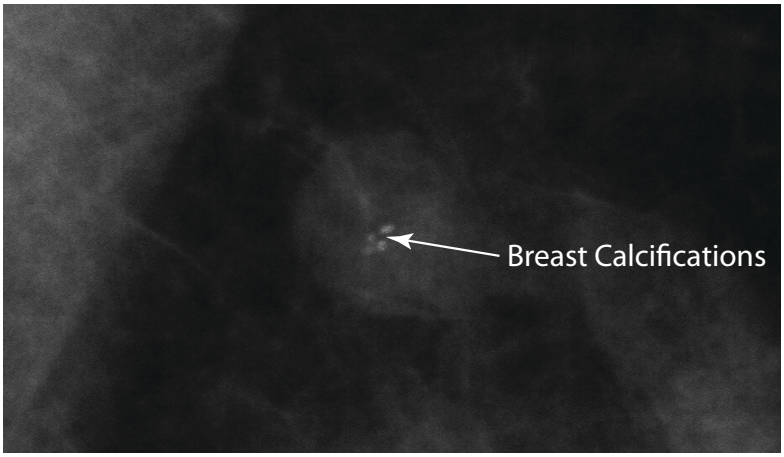

Figure 1: A mammogram showing breast calcifications as the bright spots within a cyst.

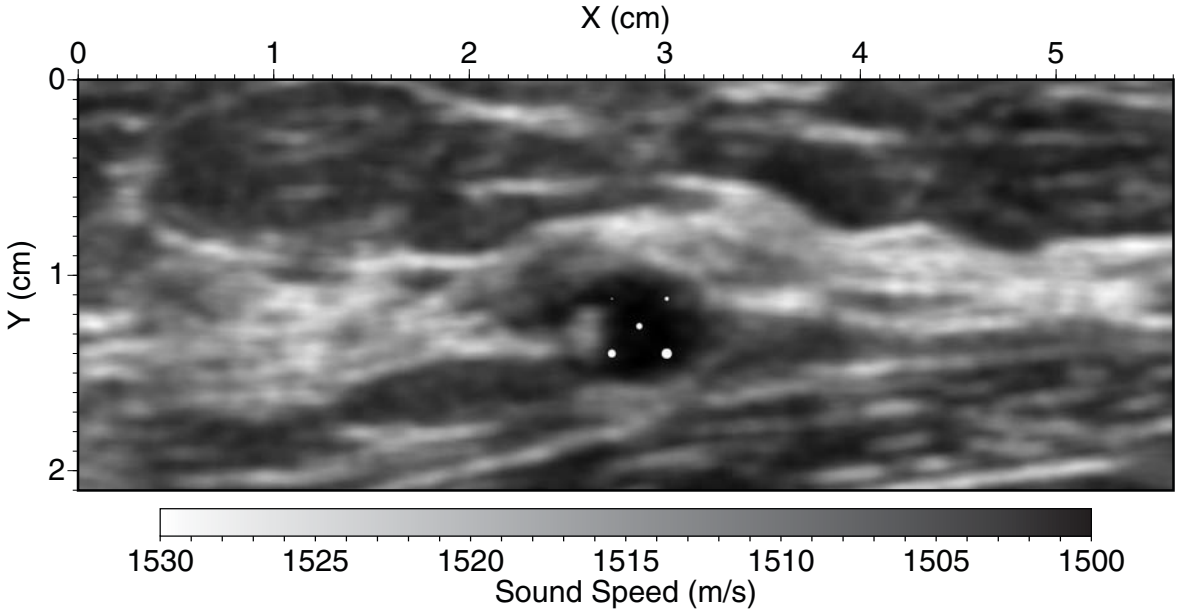

Figure 2: The sound speed profile of a numerical breast phantom containing five microcalcifications with diameters of 0.08 mm, 0.20 mm, 0.32 mm, 0.40 mm, and 0.52 mm within a cyst. The numerical phantom is constructed based on an *in vivo* ultrasound breast image. The embedded microcalcifications are shown as the bright spots.

ultrasound diffraction from embedded microcalcifications. To satisfy the spatial sampling criterion of ultrasound data (or two receivers per wavelength) to avoid image aliasing during image reconstruction, it requires at least 373 elements in the linear transducer array.

We use a staggered-grid finite-difference scheme to solve the acoustic-wave equation in heterogeneous media, and generate ultrasound scattering/diffraction data for the numerical breast phantom in Fig. 2. We then conduct super-resolution imaging with the factorization method using the synthetic ultrasound data. Figure 3(a) is the magnified view of the region with the embedded breast microcalcifications in Fig. 2. Super-resolution images of breast microcalcifications obtained with 701, 351, and 201 transducer elements (or 3.75, 1.9, and 1.1 elements per wavelength) are shown in Figs. 3(b)-(d). The microcalcifications can be clearly detected from Figs. 3(b)-(d) even though the image artifacts increase with the decreasing number of transducer elements used. The image artifacts are particularly pronounced when only 201 elements are used. An image anti-alias approach is needed for the this case to improve image quality.

We next conduct wave-equation reflection imaging. Wave-equation imaging produces images with phase that can be transformed into envelope images. Figure 4 shows our wave-equation reflection imaging results obtained using 401 and

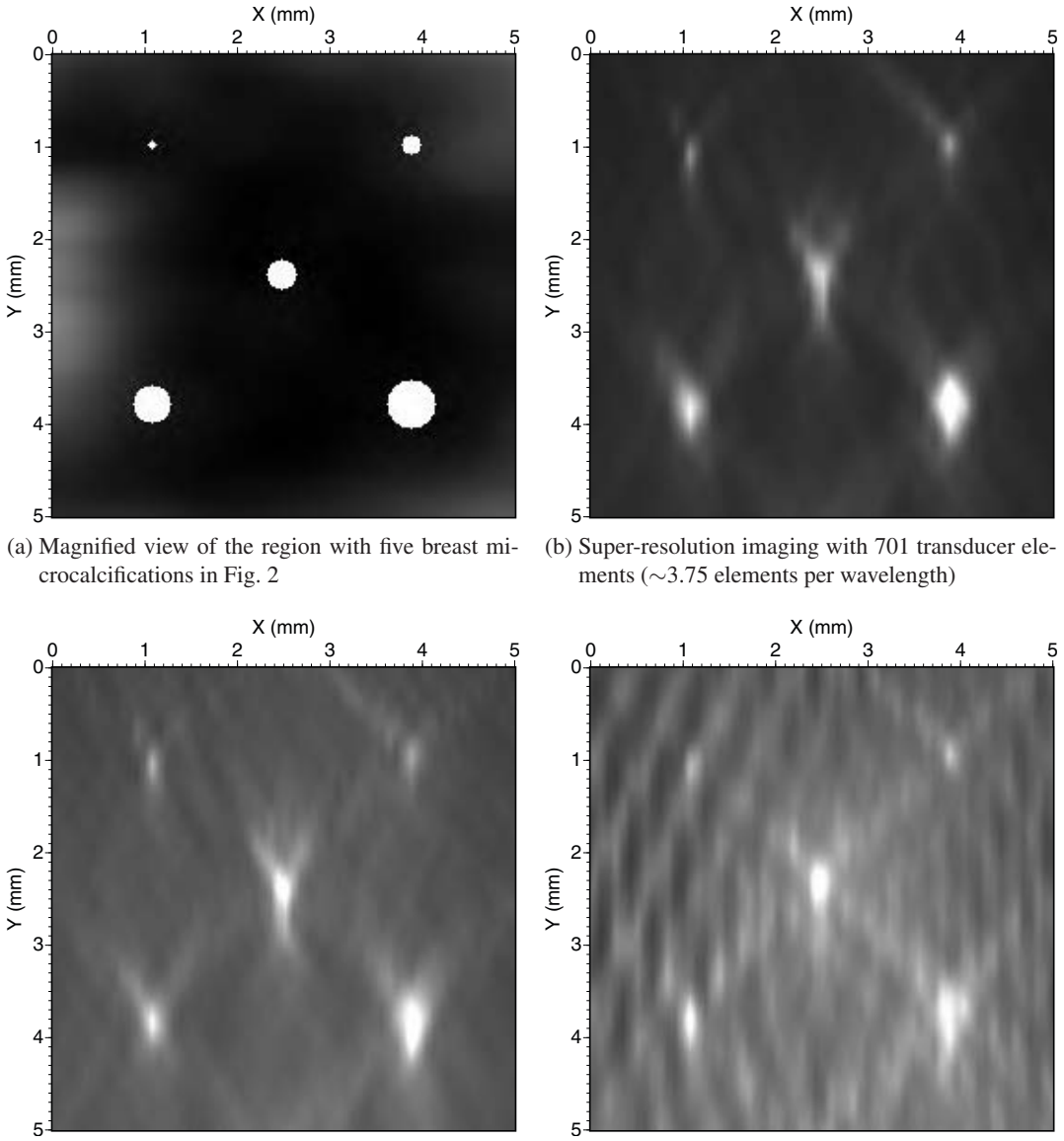

(a) Magnified view of the region with five breast microcalcifications in Fig. 2

(b) Super-resolution imaging with 701 transducer elements (∼3.75 elements per wavelength)

(c) Super-resolution imaging with 351 transducer elements (∼1.9 elements per wavelength)

(d) Super-resolution imaging with 201 transducer elements (∼1.1 elements per wavelength)

Figure 3: Magnified view of the region with embedded microcalcifications in Fig. 2 and the corresponding super-resolution imaging results with different numbers of transducer elements of the linear ultrasound array. All five microcalcifications can be clearly identified. Image artifacts increase with decreasing numbers of the transducer elements used for imaging.

201 elements. All five microcalcifications are well imaged, including their round shapes. Some weak image artifacts are caused by the limited length of the linear transducer array. This numerical example demonstrates that wave-equation reflection imaging is a powerful tool for detecting microcalcifications and reconstructing shapes of breast anomalies.

3.2 Breast microcalcifications within a cancerous mass

The numerical breast phantom in Fig. 5 is constructed from an *in vivo* image with malignant calcifications. Again, five microcalcifications with sizes ranging from 0.08 mm to 0.52 mm are embedded into the cancerous mass. We use the same finite-difference wave-equation scheme to generate synthetic data of ultrasound diffraction from the embedded microcalcifications. The size and the central frequency of the linear transducer array that scans the breast phantom at the top surface are the same as those of the previous numerical example.

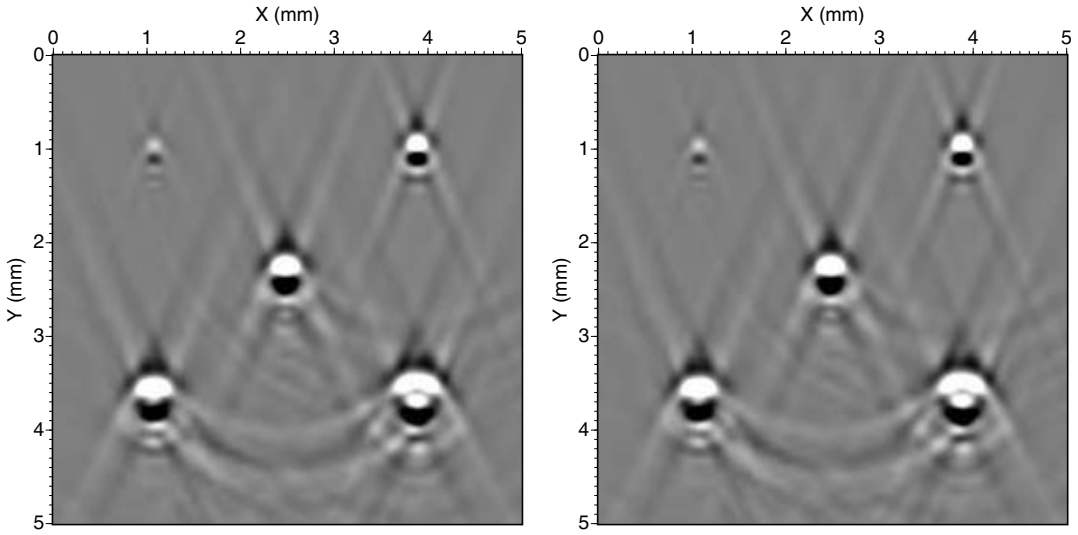

(a) Image with phase obtained using wave-equation reflection imaging with 401 transducer elements (∼2.1 elements per wavelength)

(b) Image with phase obtained using wave-equation reflection imaging with 201 transducer elements (∼1.1 elements per wavelength)

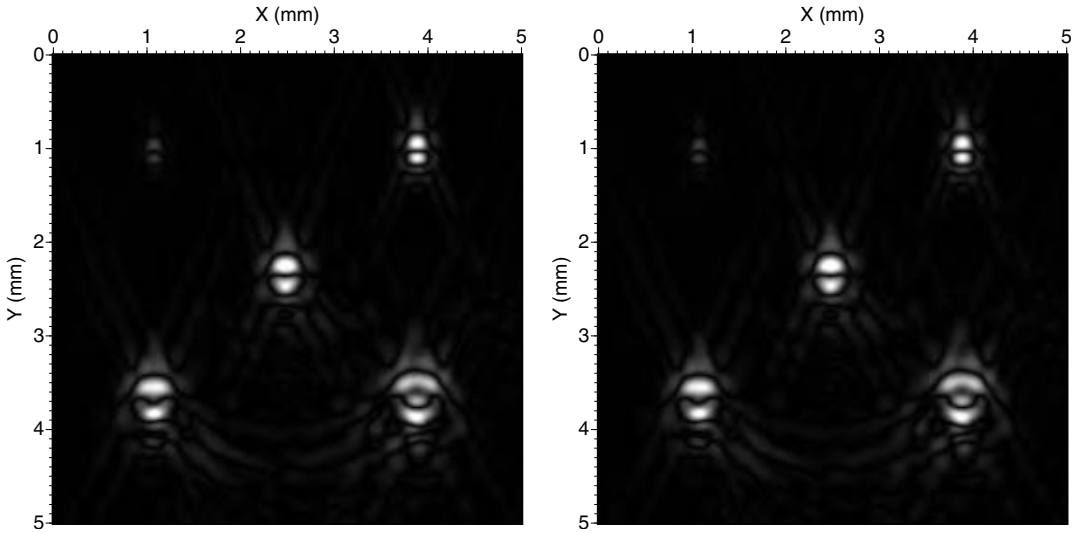

(c) Envelope image obtained using wave-equation reflection imaging with 401 transducer elements (∼2.1 elements per wavelength)

(d) Envelope image obtained using wave-equation reflection imaging with 201 transducer elements (∼1.1 elements per wavelength)

Figure 4: Wave-equation reflection imaging results with different numbers of transducer elements of the linear ultrasound array. In the images with phase in (a) and (c), the white color is for the positive image values, and the black color is for the negative image values. All five microcalcifications are well imaged, even when only 201 transducer elements are used.

We perform wave-equation reflection imaging with the synthetic ultrasound data. The magnified view of the region with the microcalcifications in Fig. 5 is shown in Fig. 6(a), and the corresponding wave-equation reflection imaging results with 401, 201, and 128 transducer elements are displayed in Figs. 6(b)-(d), respectively. All breast microcalcifications are clearly reconstructed, even when only 128 transducer elements are used. This demonstrates the robustness of wave-equation reflection imaging for microcalcification detection.

The higher the ultrasound frequency, the better is the image resolution. Our numerical imaging examples use a 5 MHz ultrasound scanner. In clinical applications, a 10 MHz ultrasound scanner can be used for breast microcalcification imaging, and the image resolution of both the super-resolution imaging and wave-equation reflection imaging could be better than

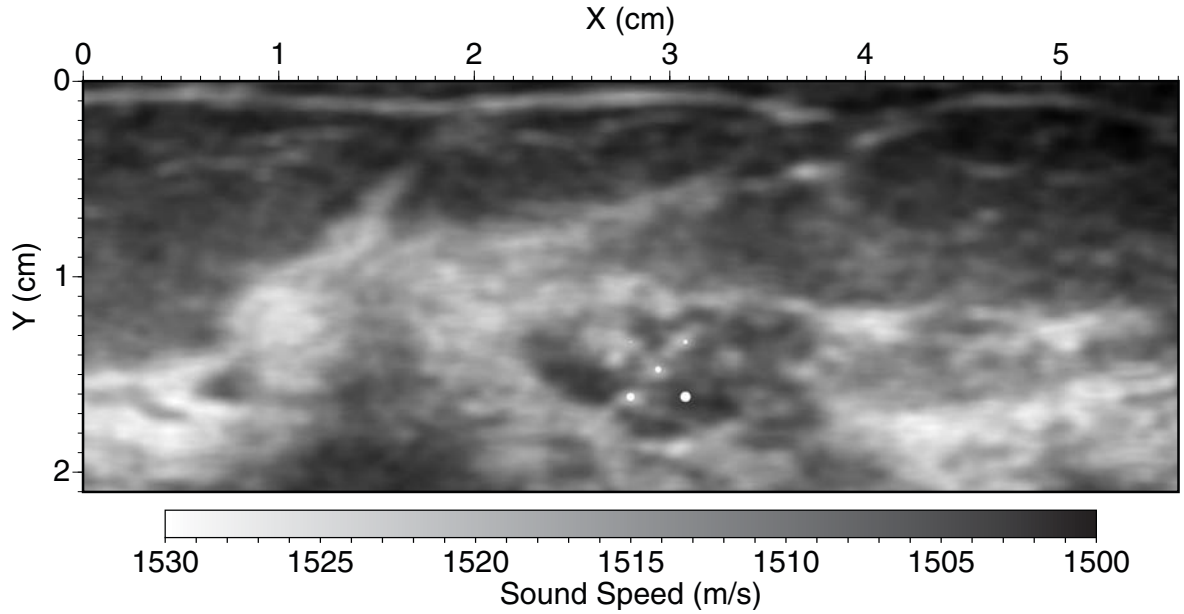

Figure 5: The sound speed profile of a numerical breast phantom containing five microcalcifications with diameters of 0.08 mm, 0.20 mm, 0.32 mm, 0.40 mm, and 0.52 mm within a cancer mass. The numerical phantom is constructed based on an *in vivo* ultrasound breast image.

the numerical examples shown in this paper. On the other hand, the data noise and three-dimensional effects of ultrasound scattering could reduce image resolution.

3.3 Image artifacts of wave-equation reflection imaging

To clearly show image artifacts of wave-equation reflection imaging, we display in Fig. 7 the images with phase for the entire breast phantom in Fig. 5 obtained using 401, 201, and 128 transducer elements. The image quality within the region containing the five breast microcalcifications in Figs. 7(a)-(c) is similar to one another, and the image artifacts appear outside that region in Figs. 7(b) and (c) when the spatial sampling criterion of ultrasound data is not satisfied. Therefore, even only using 201 or 128 transducer elements, wave-equation reflection imaging can still clearly image breast microcalcifications when they are located beneath the central region of the linear transducer array.

4. CONCLUSIONS

Breast microcalcifications cause ultrasound diffraction, and only wave-theory-based ultrasound imaging methods can properly handle ultrasound diffraction to correctly reconstruct images of microcalcifications. We have demonstrated using numerical breast phantoms that both the super-resolution imaging with the factorization method and wave-equation reflection imaging can clearly image breast microcalcifications in the heterogeneous breast. In clinical applications, a linear ultrasound transducer array consists of 128 to 512 elements. When the spatial sampling criterion of ultrasound data is not satisfied when using low numbers of elements, image artifacts could appear. An anti-alias image filter could be designed to reduce image artifacts. However, even when the criterion is not met, wave-equation reflection imaging can still clearly image breast microcalcifications if they are located beneath the central region of the linear ultrasound array. Both the super-resolution imaging with the factorization method and wave-equation reflection imaging have great potential for clinical breast microcalcification imaging.

5. ACKNOWLEDGMENTS

This work was supported through the Breast Cancer Research Program grant #BC085221 of U.S. DOD Congressionally Directed Medical Research Programs. FS and PH acknowledged the support by the UK EPSRC grant EP/F00947X/1.

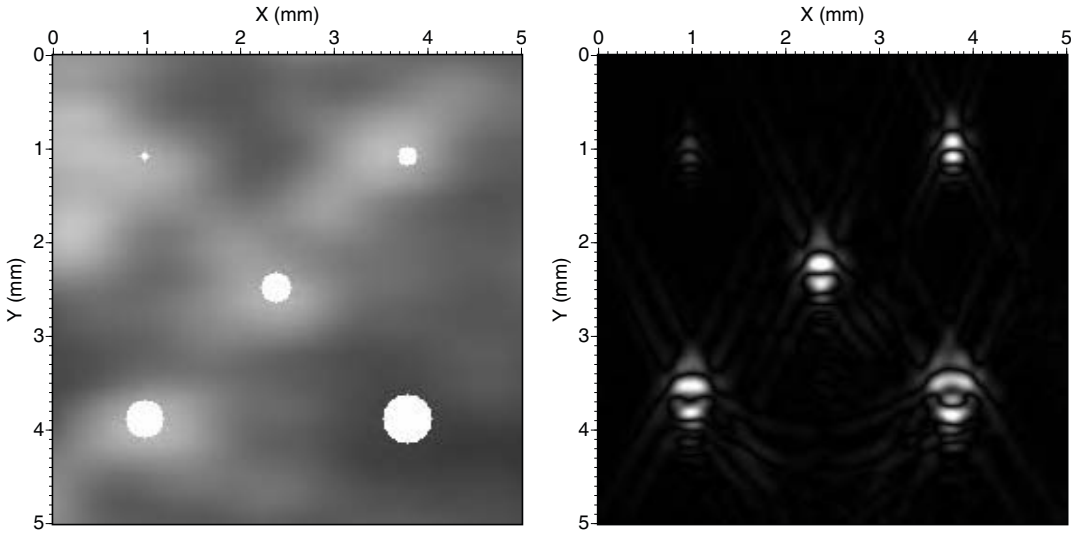

(a) Magnified view of the region with five breast microcalcifications shown in Fig. 5.

(b) Wave-equation reflection imaging with 401 transducer elements (∼2.1 elements per wavelength)

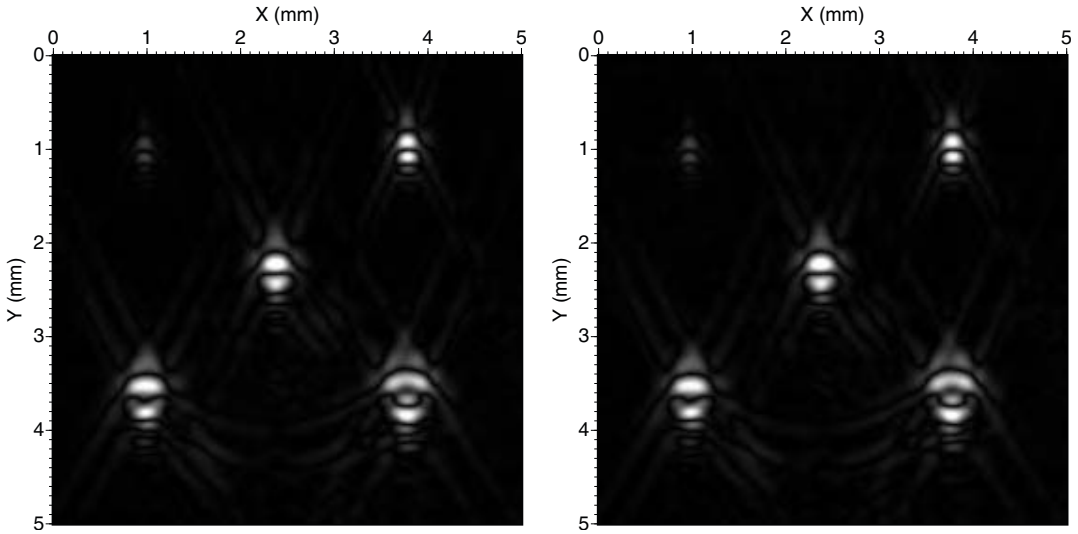

(c) Wave-equation reflection imaging with 201 transducer elements (∼1.1 elements per wavelength)

(d) Wave-equation reflection imaging with 128 transducer elements (∼0.68 elements per wavelength)

Figure 6: Magnified view of the region with embedded microcalcifications in Fig. 5 and the corresponding wave-equation reflection imaging results with different numbers of transducer elements of the linear ultrasound array. All microcalcifications are well imaged even when only 128 transducer elements are used.

REFERENCES

[1] Peart, O., [*Mammography and Breast Imaging Just the Facts*], McGraw-Hill Medical Publishing Division, New York (2005).

[2] Boccignone, G., Chianese, A., and Picariello, A., "Computer aided detection of microcalcifications in digital mammograms," *Computers in Biology and Medicine* **30**, 267–286 (2000).

[3] Arodz, T., Kurdziel, M., Popiela, T. J., Sevre, E. O. D., and Yuen, D. A., "Detection of clustered microcalcifications in small field digital mammograpy," *Computer Methods and Programs in Biomedicine* **81**, 56–65 (2006).

[4] Karssemeijer, N., Bluekens, A. M., Beijerinck, D., Deurenberg, J. J., Beekman, M., Visser, R., van Engen, R., Bartels-Kortland, A., and Broeders, M. J., "Breast cancer screening results 5 years after introduction of digital mammography in a population-based screening program," *Radiology* **253**, 353–358 (2009).

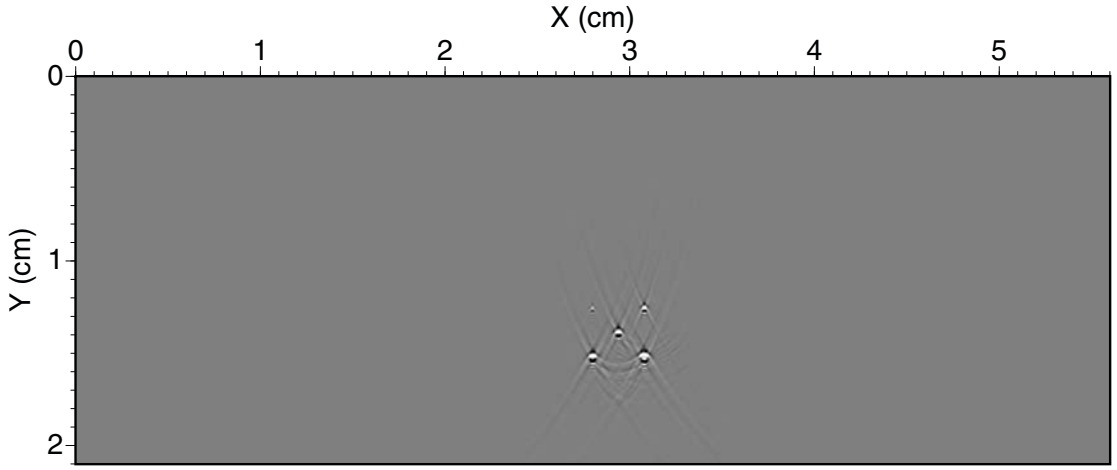

(a) Image with phase obtained with 401 transducer elements (∼2.1 elements per wavelength)

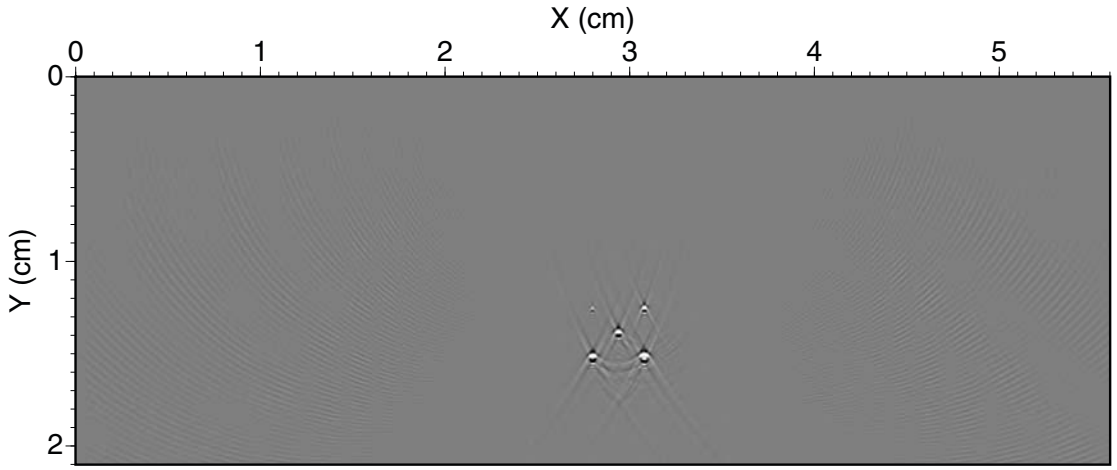

(b) Image with phase obtained with 201 transducer elements (∼1.1 elements per wavelength)

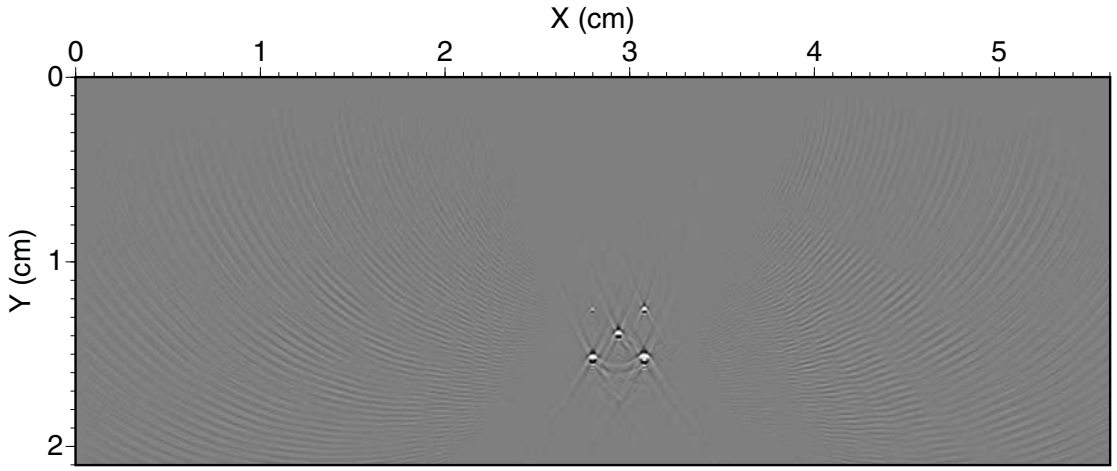

(c) Image with phase obtained with 128 transducer elements (∼0.68 elements per wavelength)

Figure 7: Comparison of images with phase for the phantom in Fig. 5 obtained using wave-equation reflection imaging with different numbers of elements in the linear transducer array. Image artifacts appear mostly outside the region with embedded breast microcalcifications when the spatial sampling criterion of ultrasound data is not satisfied in (b) and (c).

[5] Gotzsche, P. C. and Olsen, O., "Is screening for breast cancer with mammography justifiable?," *The Lancet* **355**, 129–134 (2000).
[6] Olsen, O. and Gotzsche, P. C., "Cochrane review on screening for breast cancer with mammography," *The Lancet* **358**, 1340–1342 (2001).
[7] Skaane, P. and Skjennald, A., "Screen-film mammography versus full-field digital mammography with soft-copy reading: Randomized trial in a population-based screening program — the oslo ii study," *Radiology* **232**, 197–204 (2004).
[8] Anderson, M. E., Soo, M. S., Bentley, R. C., and Trahey, G. E., "The detection of breast microcalcifications with medical ultrasound," *JASA* **101**, 29–39 (1997).
[9] Anderson, M. E., Soo, M. S. C., and Trahey, G. E., "Microcalcifications as elastic scatterers under ultrasound," *IEEE Trans. Ultrason. Ferroelectr. Freq. Control* **45**, 925–934 (1998).
[10] Alizad, A., Fatemi, M., Wold, L. E., and Greenleaf, J. F., "Performance of vibro-acoustography in detecting microcalcifications in excised human breast tissue: A study of 74 tissue samples," *IEEE Trans Med. Imaging* **23**, 307–312 (2004).
[11] Nagashima, T., Hashimoto, H., Oshida, K., Nakano, S., Tanabe, N., Nikaido, T., Koda, K., and Miyazaki, M., "Ultrasound demonstration of mammographically detected microcalcifications in patients with ductal carcinoma in situ of the breast," *Breast Cancer* **12**, 216–220 (2005).
[12] Yang, W. T., Suen, M., Ahuja, A., and Metreweli, C., "In vivo demonstration of microcalcification in breast cancer using high resolution ultrasound," *The British Journal of Radiology* **70**, 685–690 (1997).
[13] Alizad, A., Whaley, D. H., Greenleaf, J. F., and Fatemi, M., "Critical issues in breast imaging by vibro-acoustography," *Ultrasonics* **44**, e217–e220 (2006).
[14] Simonetti, F., "Multiple scattering: The key to unravel the subwavelength world from the far-field pattern of a scattered wave," *Physical Review E* **73**, 036619–1–13 (2006).
[15] Simonetti, F., Huang, L., Duric, N., and Rama, O., "Imaging beyond the born approximation: An experimental investigation with an ultrasonic ring array," *Physical Review E* **76**, 036601–1–10 (2007).
[16] Kirsch, A., "Characterization of the shape of a scattering obstacle using the spectral data of the far field operator," *Inverse Problems* **14**, 1489–1512 (1998).
[17] Huang, L., Duric, N., and Littrup, P., "Ultrasonic breast imaging using a wave-equation migration method," *Proc. SPIE* **5035**, 432–439 (2003).
[18] Huang, L., Duric, N., and Littrup, P., "Breast imaging with time-reversed ultrasound," *Proc. SPIE* **6147**, 156–167 (2006).
[19] Huang, L. and Quan, Y., "Ultrasound pulse-echo imaging using the split-step Fourier propagator," *Proc. SPIE* **6513**, 651305–1–12 (2007).
[20] Huang, L., Hanson, K. M., Quan, Y., Li, C., and Duric, N., "Globally optimized Fourier finite-difference method for ultrasound breast imaging," *Proc. SPIE* **6920**, 692007–1–11 (2008).
[21] Li, C., Duric, N., Littrup, P., and Huang, L., "In vivo breast sound-speed imaging with ultrasound tomography," *Untrasound in Med. & Biol.* **35**, 1615–1628 (2009).